3.
A SINGLE SIDED MEANDERED DUAL ANTENNA STRUCTURE FOR UHF RFID TAGS

3.1. Introduction

Recently, the application of Radio Frequency Identification (RFID) systems became more popular in different sectors such as industries, distribution logistics, libraries, and merchandise [Xiao *et al*. (2007), Wu *et al.* (1999)]. The basic function of RFID systems is to retrieve automatically the information through a reader that has been previously inserted in a passive tag [Lahiri (2005), Lozani and Nieto (2011)].

For various application purposes, RFID tags need to be small. To meet these requirements, several RFID tag antennas have been proposed that operate in UHF band. Some compact antenna structures have been reported using inductively coupled structure [Son and Pyo (2005), Kim *et al.* (2008), Chen and Tsao (2010), Kim *et al.* (2011), Sun *et al.* (2013)], inverted-F [Soras *et al*. (2002), Hirvonen *et al.* (2004)], meandered antenna [Bae *et al*. (2008), Chen *et al.* (2011)a, Soliman *et al*. (2012)], and some other techniques [Marrocco, (2008), Chen *et al*. (2011)a, Naji and Fyath (2013)]. In [Kim *et al.* (2011), Son and Pyo (2005), Sun *et al.* (2013), Chen and Tsao (2010), Kim *et al.* (2008), Soras *et al*. (2002), Hirvonen *et al.* (2004), Soliman *et al*. (2012), Bae *et al*. (2008)] utilizes conventional single antenna structure while some other utilizes dual antenna structure [Chen *et al*. (2011)a, Chen *et al.* (2011)b, Naji and Fyath (2013)].

Since the conventional single antenna element RFID tag uses a single antenna for both the receiving and backscattering, it has some inherent limitations. The tag chip alternatively changes its impedances between highly complex values which are complex conjugate matched to antenna impedance and a short circuit value. During the short circuit, the antenna will not receive any power (continuous wave) from the reader; therefore, the efficiency of the energy absorption drops significantly in this phase. Further, the two impedance conditions, short circuit and conjugate matched, would not provide the maximum impedance difference in

the backscattered signals which results in shorter read range. To mitigate the limitations of the conventional single antenna structure, RFID tags with dual antenna structures have been reported. In [Chen *et al.* (2011)a] and [Chen *et al.* (2011)b], the dual antenna structure is proposed with two meandered line antennas placed on the both sides of the substrate and operating in UHF bands. Whereas in [Naji and Fyath (2013)] dual fractal antenna structure has been proposed to operate at 5.8 GHz and printed on both sides of the substrate. Since both the antennas reported in [Chen *et al.* (2011)a] and [Naji and Fyath (2013)] are placed on the either sides of the substrate, then it is very difficult to use these tag antennas on the metallic surfaces and they do not have high differential radar cross section (ΔRCS) and gain. Therefore, it is highly desirable to design an easy to fabricate RFID tag antenna that can mitigate these limitations.

In this chapter, a single sided novel dual antenna structure for UHF RFID tag with significant enhancement in read range is proposed. The proposed tag consists of two independent antennas. One antenna is exclusively used for receiving and the other for backscattering. This technique provides the maximum and continuous power supply along with maximum difference level of RCS in the backscattering mode, simultaneously. The performance of the proposed antenna is evaluated on the basis of differential RCS and read range. Table 3.1 summarizes the performance comparison such as size, operating frequency, improvement in read range, increased RCS, and type of antenna structure. It is observed that proposed easy to fabricate single sided antenna structure has significant enhancement of read range and ΔRCS with respect to conventional tag antenna as compared to the other antenna structure at the cost of some increase in size. The concepts of dual antenna structure along with antenna design are discussed in the following sections of the manuscript with the simulated and measured results.

Table 3.1: Comparison of reported dual antenna structure for RFID applications

References	Antenna Size (mm^2)	Frequency (GHz)	Improved in Read Range* (m)	Increased ΔRCS (dBsm)	Antenna Structure
[chen *et al*. (2011)a], [chen *et al*. (2011)b]	32.8×32.8	0.915	0.3	22	Double sided
[Naji and Fyath (2013)]	13.9×13.2	5.8	0.6	Not provided	Double sided
Proposed	50×67	0.925	2	88	Single sided

* As compared with the convention tag antenna of the same authors'

3.2. Antenna configuration

The configuration and fabricated prototype of the proposed antenna for RFID tag are shown in Figure 3.1. It is fabricated on low cost FR4 substrate having dielectric constant ($_r$) 4.4, loss tangent of 0.018, thickness 1.6 mm, and overall size 50 mm × 67 mm. The proposed dual antenna consists of two independent antennas. One is made up of a meandered radiating element inductively coupled with a small rectangular loop as a feeding element which acts as receiving antenna. Whereas, the other one is meandered dipole antenna, along with a parasitic strip which acts as backscattering antenna. The design concept of the proposed antenna in receiving mode is based on the paper reported in [Chen *et al*. (2011)a].

The coupling strength of receiving antenna is controlled by the distance between the rectangular loop and the radiating element. Figure 3.2 shows the equivalent circuit of the inductively coupled feed structure. The inductive coupling is modeled by a transformer.

The input impedance of the receiving antenna (Z_a) is given by, [Son and Pyo (2005), Sun *et al*. (2013)]

$$Z_a = R_a + jX_a = Z_{loop} + \frac{(2\pi fM)^2}{Z_r} \tag{3.1}$$

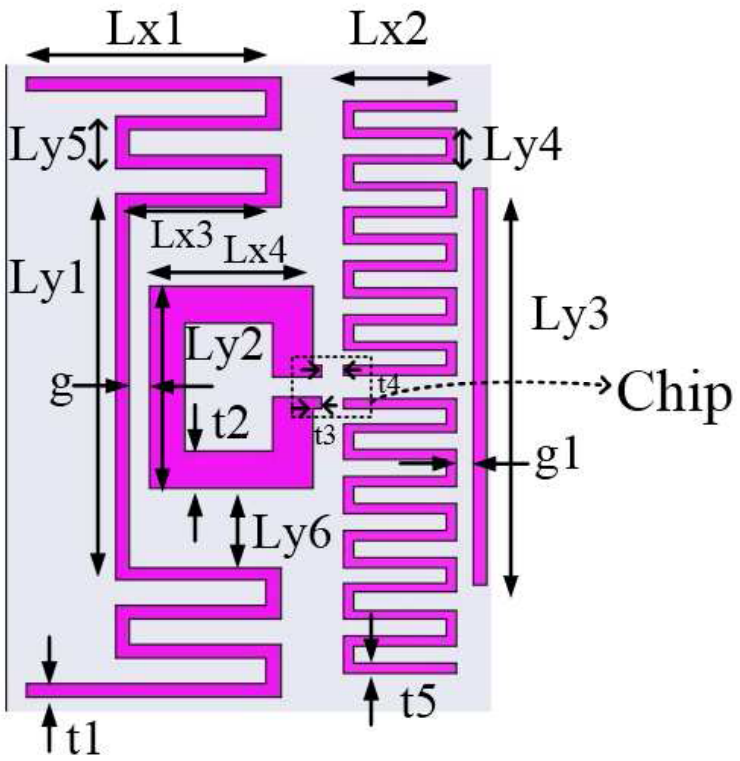

(a)

(b)

Figure 3.1: (a) Geometry and (b) fabricated proposed dual tag antenna

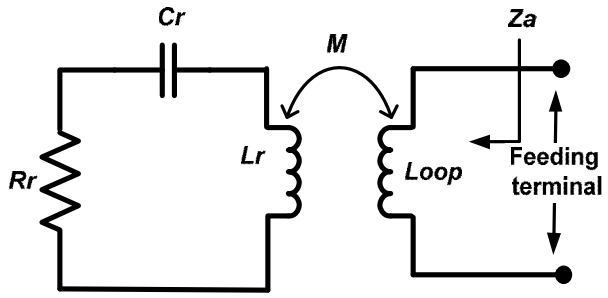

Figure 3.2: Equivalent circuit of the inductively coupled feed structure.

$$R_a = \frac{(2\pi fM)^2}{R_r} \tag{3.2}$$

$$X_a = 2\pi fL_{loop} \tag{3.3}$$

From equations (3.1)-(3.3), it is observed that R_a, M, and X_a are the functions of L_{loop}, so they are separately controllable and could be adjusted for different RFID chips with different input impedances.

3.3. Results and discussion

The proposed antenna is designed for Alien IC Higgs tag chip which has an input impedance of 13.5-j110 Ω at 925 MHz [*Higgs 4 product overview, Alien Technology*, 2012]. All the simulations are performed using the Ansys high frequency structure simulator (HFSS) [HFSS ver. 14.0] that uses Finite Element Method (FEM) as the numerical technique to solve the EM problems. The optimized values of shape parameters of the proposed antenna are shown in Table 3.2.

Table 3.2: Dimension of proposed antenna structure

Antenna parameter	Value (mm)	Antenna parameter	Value (mm)	Antenna parameter	Value (mm)	Antenna parameter	Value (mm)
Lx1	26	Ly1	40	Ly5	5.5	t2	3.75
Lx2	11.5	Ly2	20.75	Ly6	10.25	t3	1
Lx3	15.5	Ly3	41	t1	1.5	t4	2.25
Lx4	16.75	Ly4	3.75	g	2	g1	1.75
t5	1						

3.3.1. Parametric study

3.3.1.1. *Receiving antenna*

The main objective of the parametric study of the receiving antenna in the presence of backscattering antenna is to achieve proper complex conjugate of the chip. To achieve complex conjugate of the chip, at a time one of the shape parameter of the receiving antenna is varied by keeping other shape parameters are fixed at their optimized value as shown in Table 3.2. To achieve these optimized values, initially coarse design of the antenna is considered based on the half wavelength concept of the radiating element.

Variation of simulated power reflection coefficient, real and imaginary parts of the input impedance of the receiving antenna and that of the chip by tuning the Lx1 by keeping other parameters constant at their optimized values, are shown in Figures 3.3(a), 3.3(b), and 3.3(c), respectively. It is observed that at the frequency of 925 MHz, the real part of the input impedance of the receiving antenna is tunable between 24.4 to 8.4 ohms, while the imaginary part is varies from 109 to 113 ohm for the variation of the Lx1.

Further, coupling length Ly2 is varied to optimize the input impedance of the receiving antenna to the complex conjugate of the chip impedance by keeping other parameters constant at their optimized values as depicted in Figure 3.4. It is observed that, at the frequency of 925 MHz, the imaginary part of the input impedance of receiving antenna is tunable from 88 to 141 ohms, whereas little variations of 8 to 18 ohms are observed in the real part. Similar effect is also observed by varying the separation ‘g’ between the meandered radiating element and a rectangular loop which is shown in the Figure 3.5.

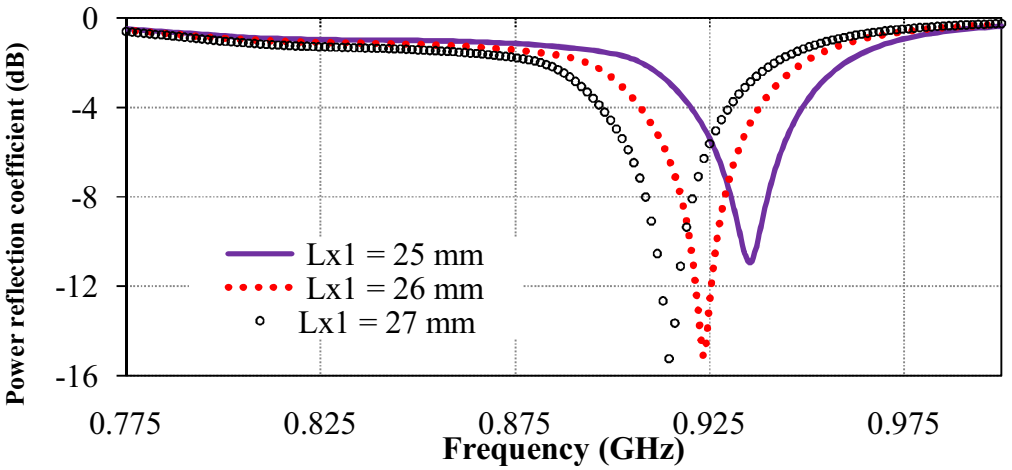

(a)

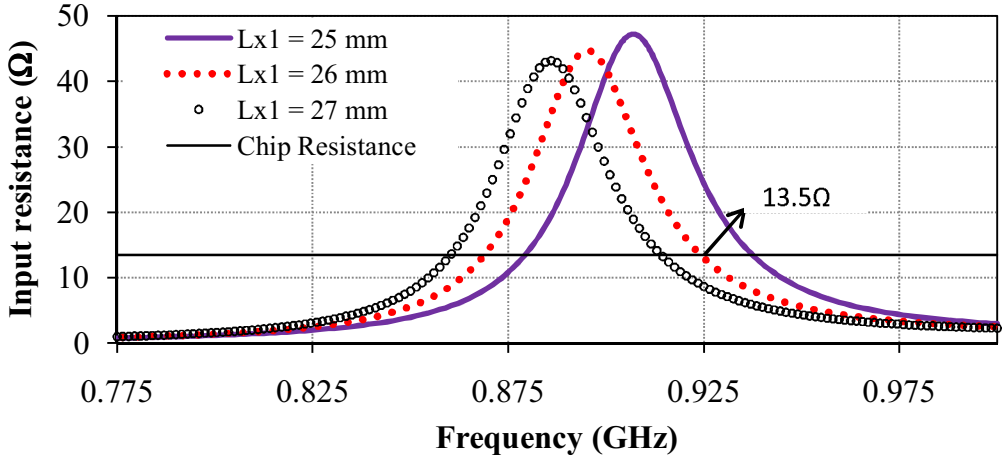

(b)

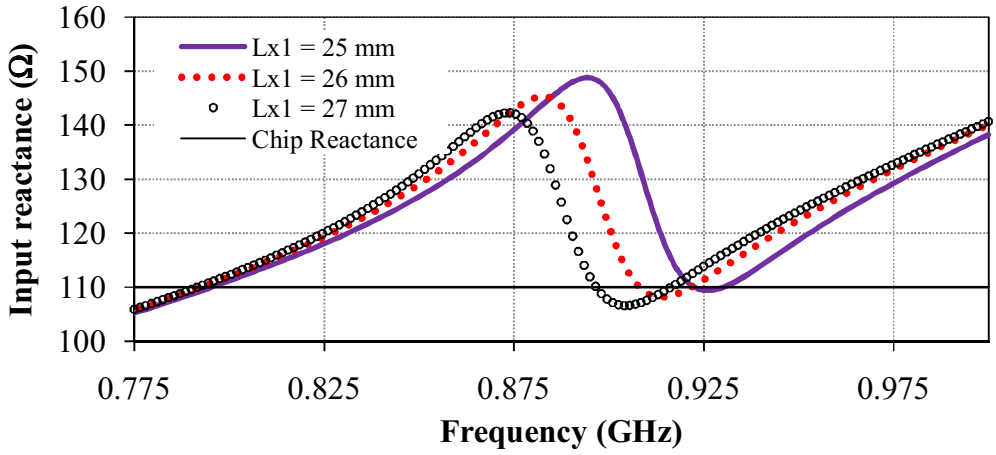

(c)

Figure 3.3: Simulated (a) power reflection coefficient, (b) real part of input impedance, (c) imaginary part of input impedance of receiving antenna by tuning the Lx1.

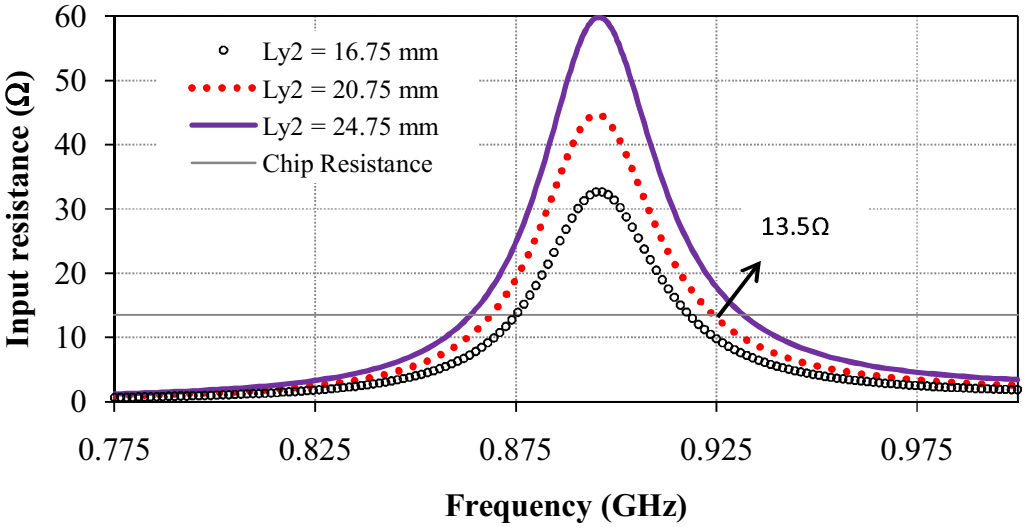

(a)

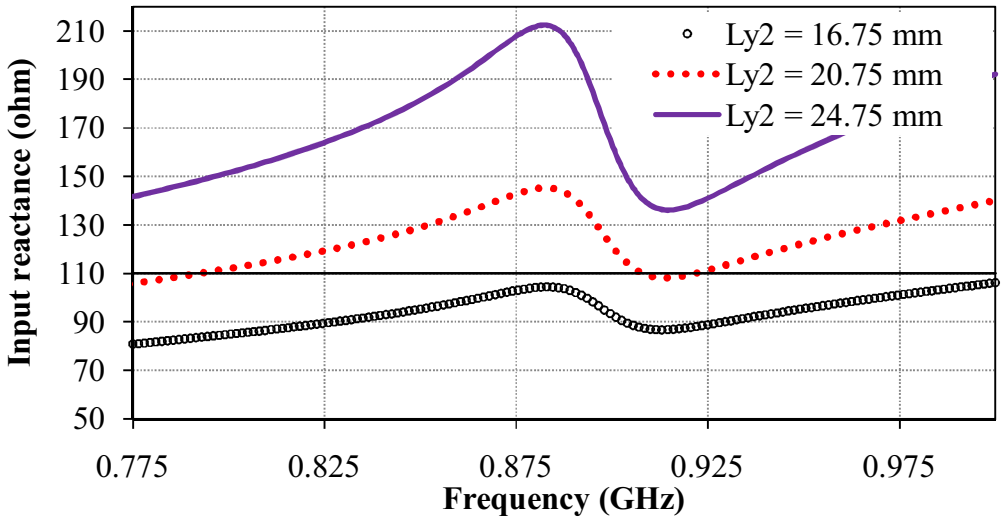

(b)

Figure 3.4: Simulated (a) real part and (b) imaginary part of input impedance of receiving antenna by tuning Ly2.

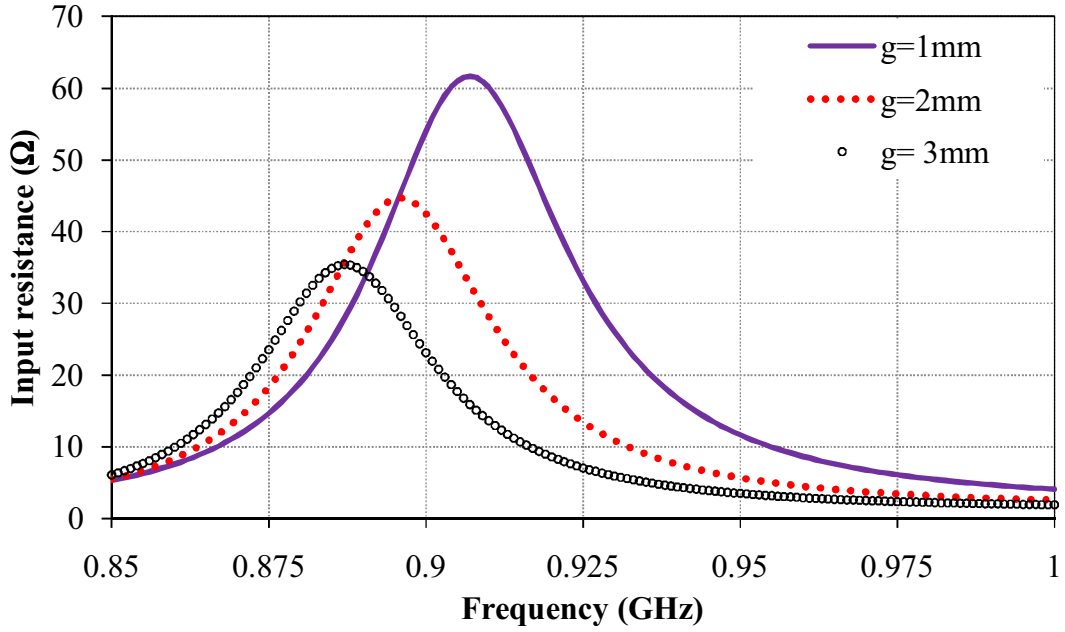

(a)

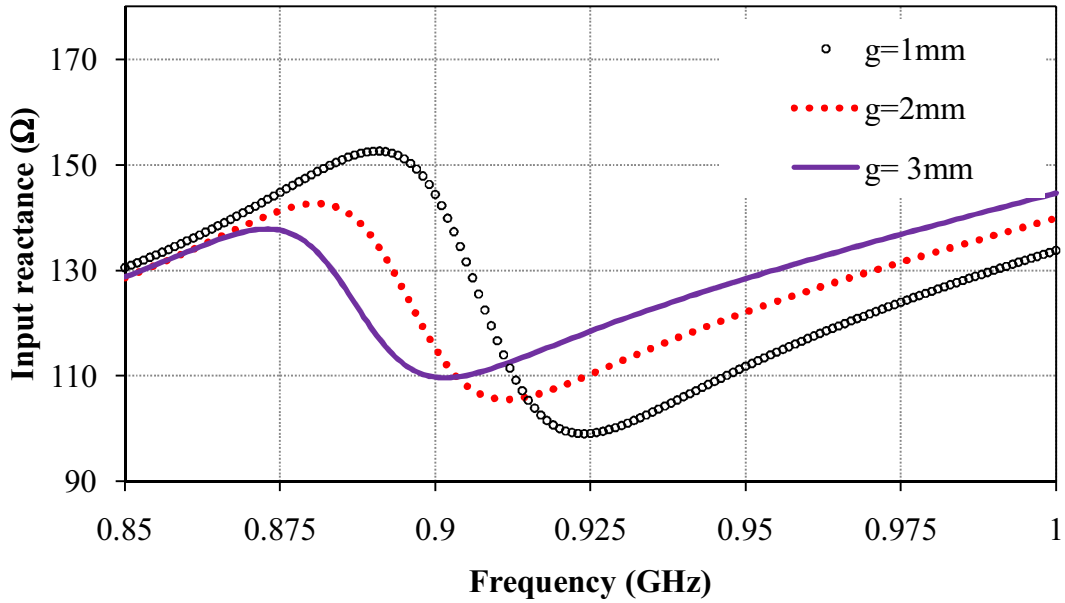

(b)

Figure 3.5: Simulated (a) real part and (b) imaginary part of input impedance of receiving antenna by tuning '*g*'.

The thickness of the meandered radiating structure (t1) and rectangular loop (t2) also show significant effect on the input impedance characteristics of the receiving antenna which is shown in Figures 3.6 and 3.7, respectively. It is observed from Figure 3.6 that the real and imaginary part of the input impedance of receiving antenna change significantly by varying a small value of t1 at 925

MHz frequency. While in Figure 3.7, imaginary part of the input impedance of receiving antenna changes significantly while little variation is observed in real part of the input impedance by changing small variation in t2.

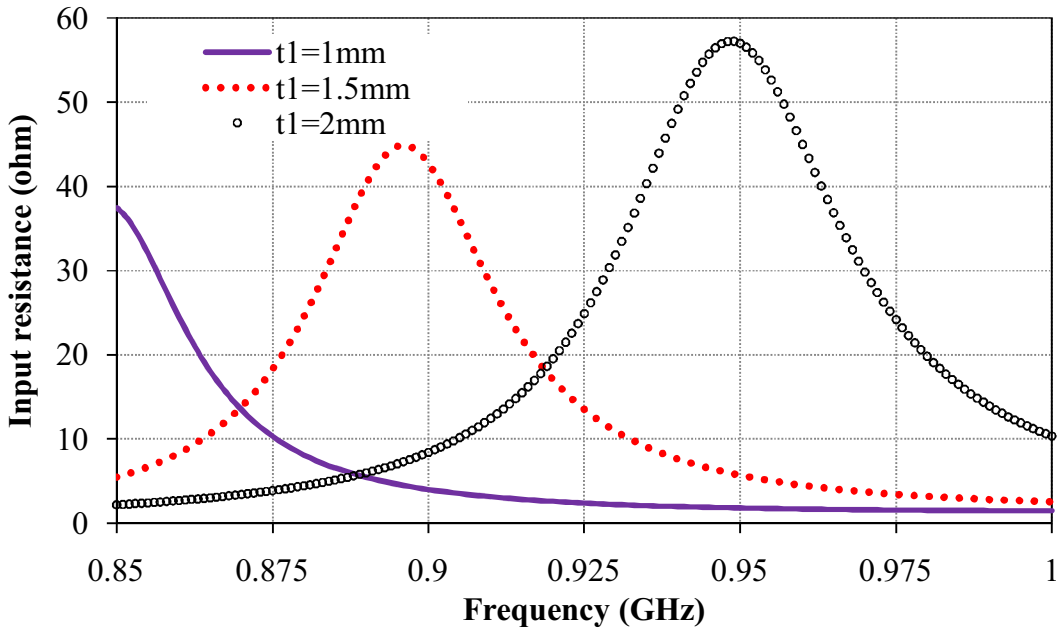

(a)

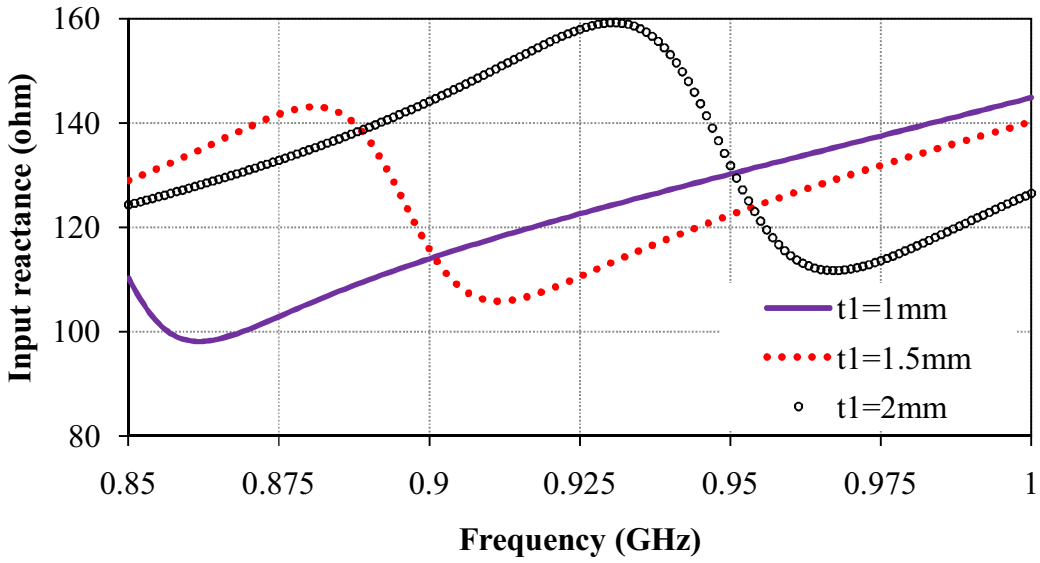

(b)

Figure 3.6: Simulated (a) real and (b) imaginary parts of input impedance of receiving antenna by tuning t1.

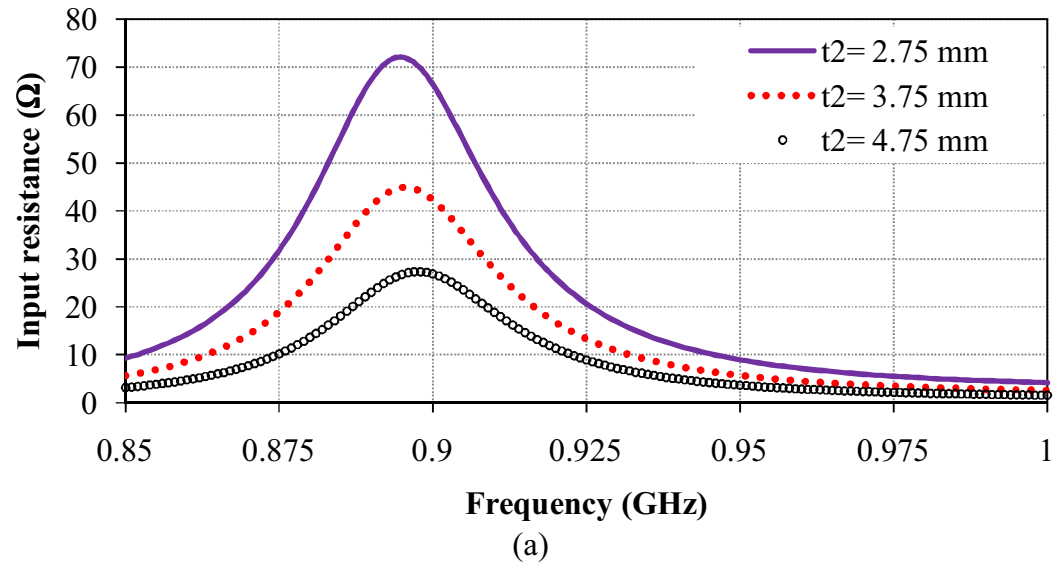

(a)

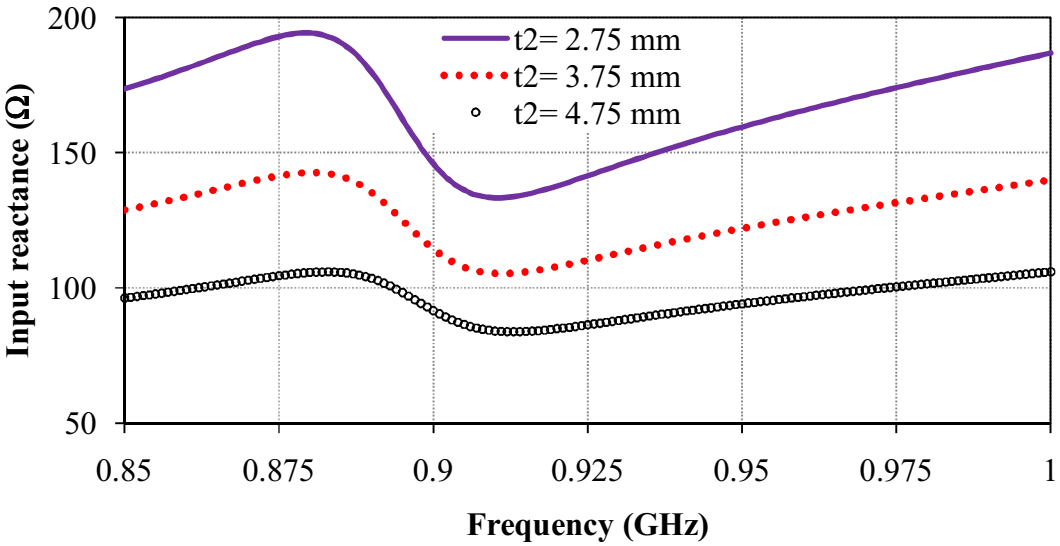

(b)

Figure 3.7: Simulated (a) real and (b) imaginary parts of input impedance of receiving antenna by tuning t2.

Further, Figures 3.8(a) and 3.8(b) show the real and imaginary part of the input impedance of the receiving antenna respectively by tuning the Ly1 by keeping optimized values of other parameters. It is observed that the Ly1 helps in fine tuning of the real and imaginary parts of the input impedance of the antenna at 925 MHz frequency. Similar effect is also observed by varying the Ly5. For the brevity the results are not shown here.

Rigorous analysis is carried out on the other shape parameters (presented in Table 3.2) of the receiving antenna to achieve the complex conjugate value of the chip impedance. After optimization, the input impedance of the receiving antenna is obtained 13 + j111 Ω at 925 MHz frequency which is close to the complex conjugate of the chip impedance (13.5-j110 ohm) by choosing the optimized values of the various shape parameters of the antenna. The proper impedance value of the antenna is required to minimize the reflection losses between the antenna and chip, and hence, improve the transmitted power and maximize the read range.

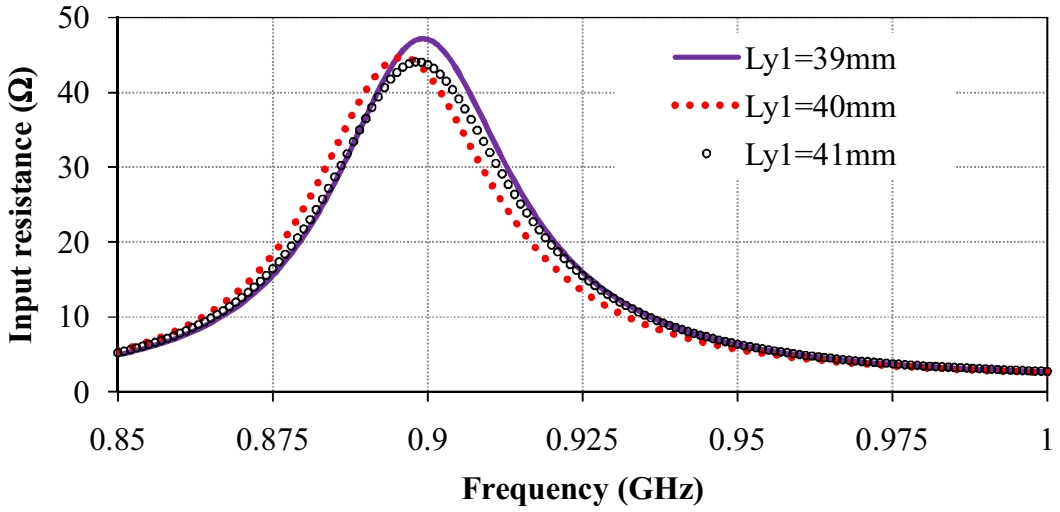

(a)

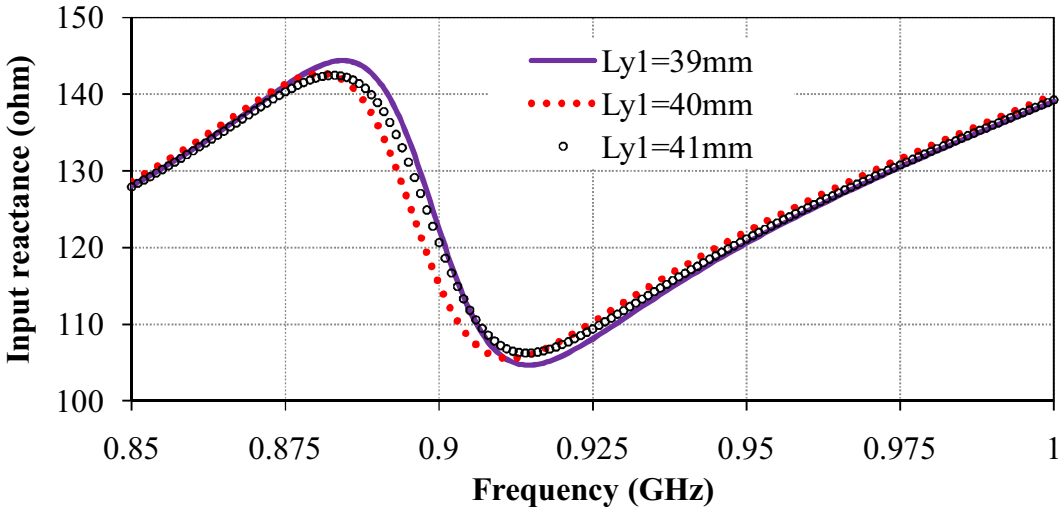

(b)

Figure 3.8: Simulated (a) real part and (b) imaginary part of input impedance of receiving antenna by tuning Ly1.

3.3.1.2. *Backscattering antenna*

The parametric study of the backscattering antenna is carried out in the presence of the receiving antenna under the complex conjugate matched condition at operating frequency. The shape parameters of the backscattering antenna are optimized in such a way that to satisfy the equation 2.6 so that in the backscattering mode, the imaginary part of the backscattering antenna should be close to zero for achieving maximum differential.

Figures 3.9 (a-e) show the variations of the imaginary part of the input impedance of the backscattering antenna with the frequency under the matched receiving antenna condition, by tuning (at a time one parameter) Ly3, g1, Lx2, Ly4 and t5 respectively, and keeping optimized values of the other parameters. It is observed that in all the cases the zero reactance value of the backscatter antenna is observed for optimized shape parameters which satisfy the equation 2.6. It indicates that the backscatter antenna properly works in the backscattering mode of the RFID tag.

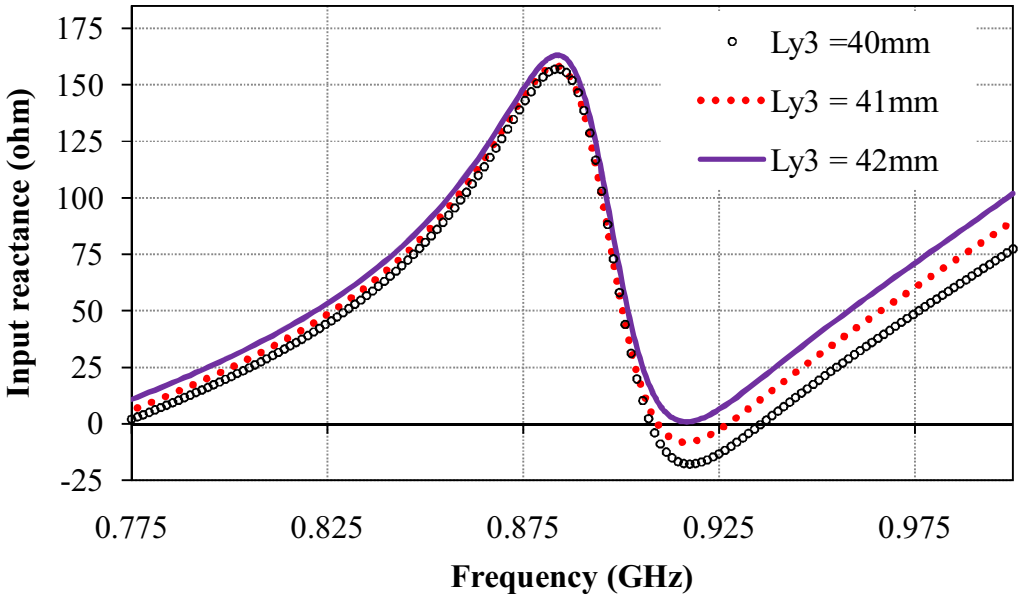

(a)

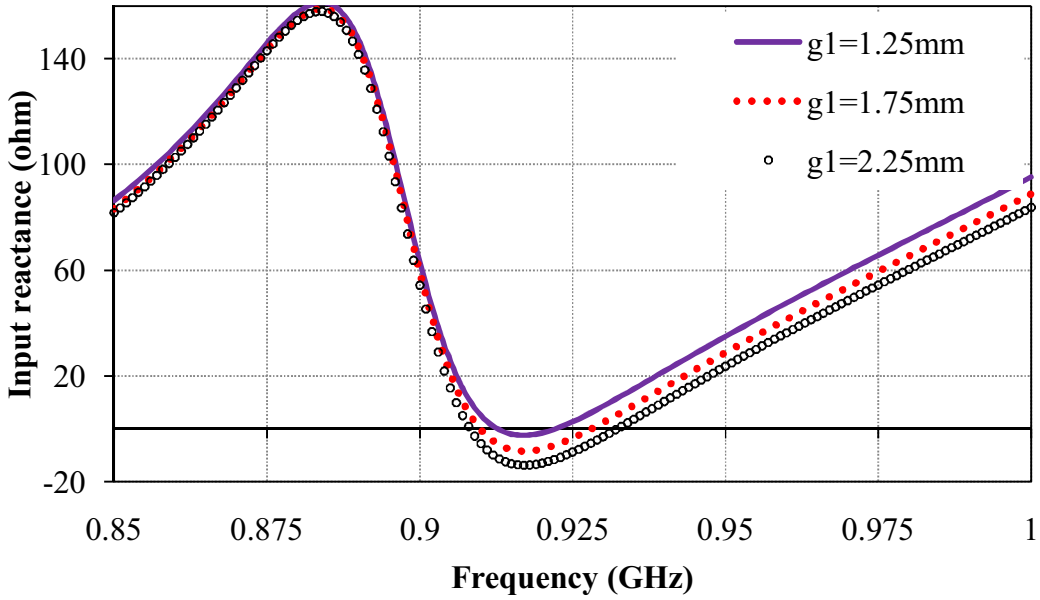
g1=1.25mm
g1=1.75mm
g1=2.25mm
Input reactance (ohm)
140
100
60
20
-20
0.85
0.875
0.9
0.925
0.95
0.975
1
Frequency (GHz)

(b)

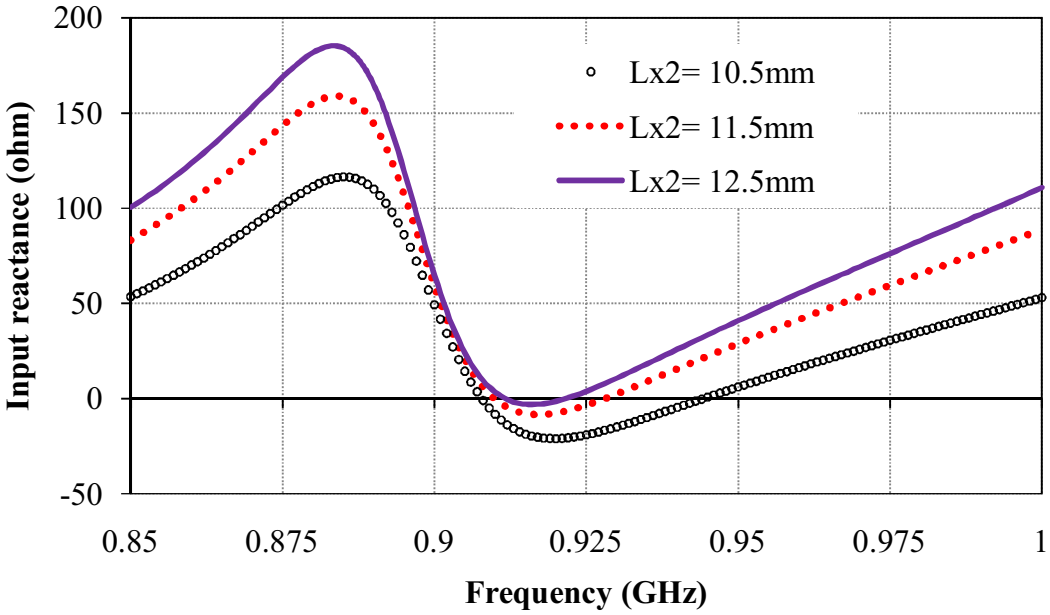
Lx2= 10.5mm
Lx2= 11.5mm
Lx2= 12.5mm
Input reactance (ohm)
200
150
100
50
0
-50
0.85
0.875
0.9
0.925
0.95
0.975
1
Frequency (GHz)

(c)

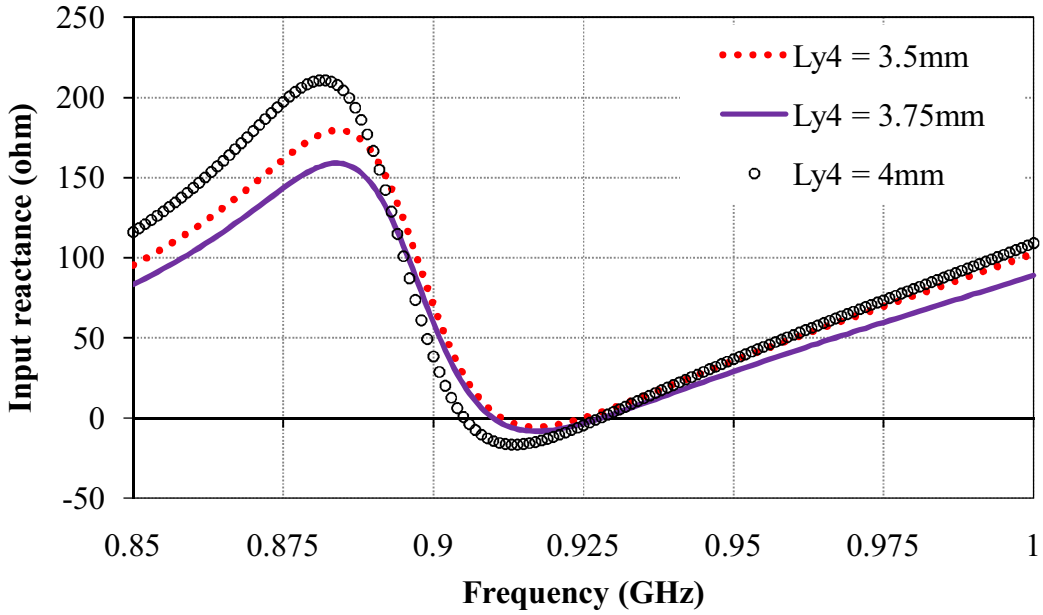

(d)

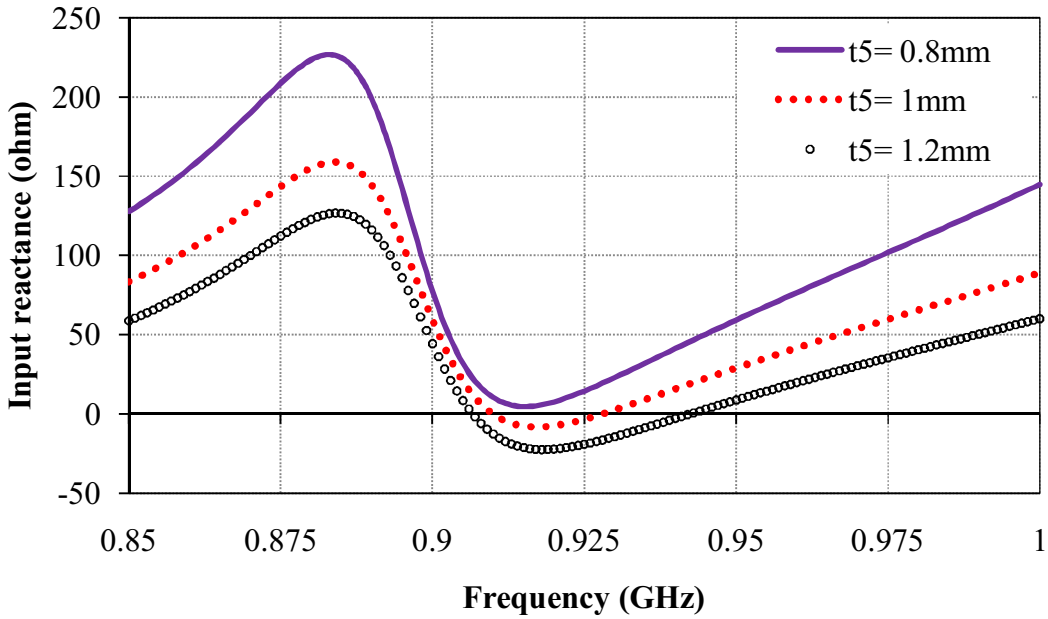

(e)

Figure 3.9: imaginary part of input impedance of backscattering antenna by tuning (a) Ly3, (b) g1, (c) Lx2, (d) Ly4 and (e) t5 when receiving antenna is matched.

3.3.2. Measurement of RFID tag antenna

To measure the characteristics of the proposed RFID tag antennas differential probe technique described in chapter 2 is used. The differential probe is fabricated as depicted in chapter 2. Figure 3.10 shows the differential probe with measurement setup. With the help of differential probe connected to the terminals of antenna, *S*-parameters for two ports of differential probe are measured. Using the values of the *S*-parameters, differential input impedance is calculated using equation 2.15. Further, with the help of differential input impedance, power reflection coefficient is calculated as [Nikitin *et al.* (2005)].

$$\Gamma(Z_L) = \frac{(Z_L - Z_a^*)}{(Z_L + Z_a)} \tag{3.4}$$

where, Z_L is the impedance of chip, Z_a is the input impedance of antenna and Z_a^* is complex conjugate of antenna's impedance.

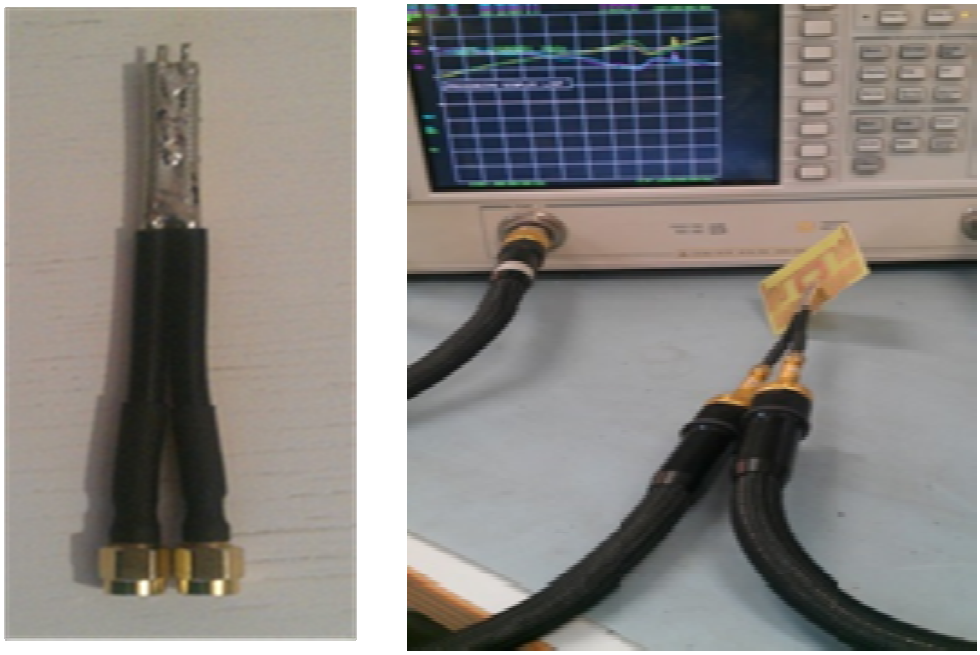

Figure 3.10: Differential probe with measurement setup

Figure 3.11(a) and 3.11(b) shows the simulated and measured results of power reflection coefficient and input impedance of receiving antenna, respectively. The simulated and measured complex input impedance of the receiving antennas is found to be 13.01 + j111.37 Ω and 13 + j109 Ω, respectively; which is close to the complex conjugate of the chip impedance i.e. (13.5 + j110 Ω). Due to the good impedance matching, low value of the power reflection coefficient is observed at 0.925 GHz which shows antenna is working properly.

The simulated and measured input reactance of backscatter antenna is shown in Figure 3.12. The measured reactance value of the backscattering antenna is observed as -2.4 Ω which is close to zero at 0.925 GHz which shows antenna is working properly. The simulated and measured results are in good agreement.

RCS of the proposed dual antenna is compared with conventional single antenna structure in Figures 3.13(a) and 3.13(b). It is observed that the differential RCS ($\Delta\sigma$) in open and short circuit states of the proposed dual-antenna structure is increased. Since the read range is directly proportional to the differential RCS under the two loading impedance, it results in the enhancement of read range, as shown in Figure 3.14. With the help of the dual antenna structure, maximize the quantity of $\Delta\sigma$ from 12 to 110 dBsm which results in increased read range from 2.4 to 4.4 m. It is noted that the receiving antenna of proposed dual-antenna structure is conjugate matched with the chip whereas; the backscatter antenna alternatively switches between open and short circuit states.

The simulated radiation pattern in terms of realized gain for the receiving and backscattering antenna in *xz*- and *yz*-plane at 925 MHz is presented in Figure 3.15. Both the antennas of the RFID tag show the omnidirectional pattern as required by the short range communication devices, with dumbbell shaped variation in *xz*-plane and nearly non-directional variation in *yz*-plane. The back scattering antenna has deep null in *xz*-plane and more variation in *yz*-plane than the receiving antenna.

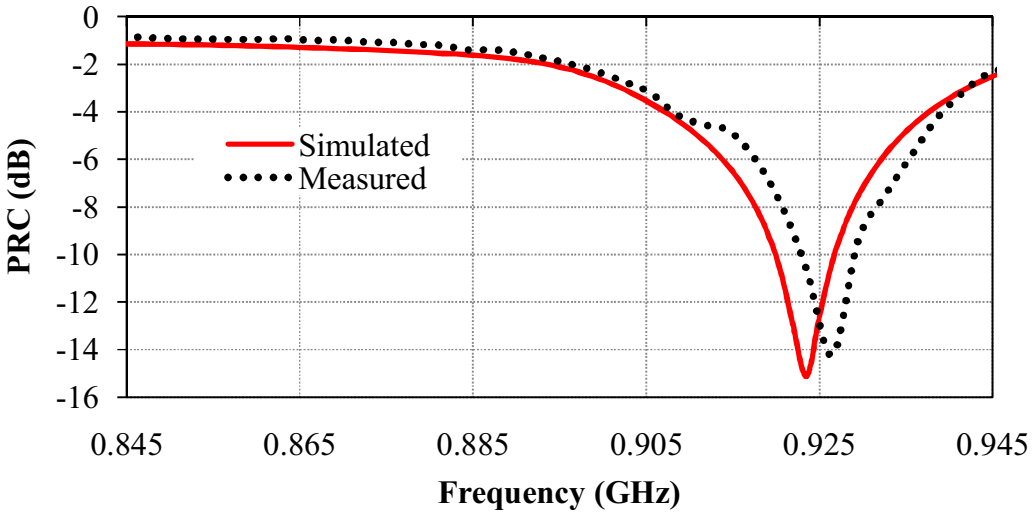

(a)

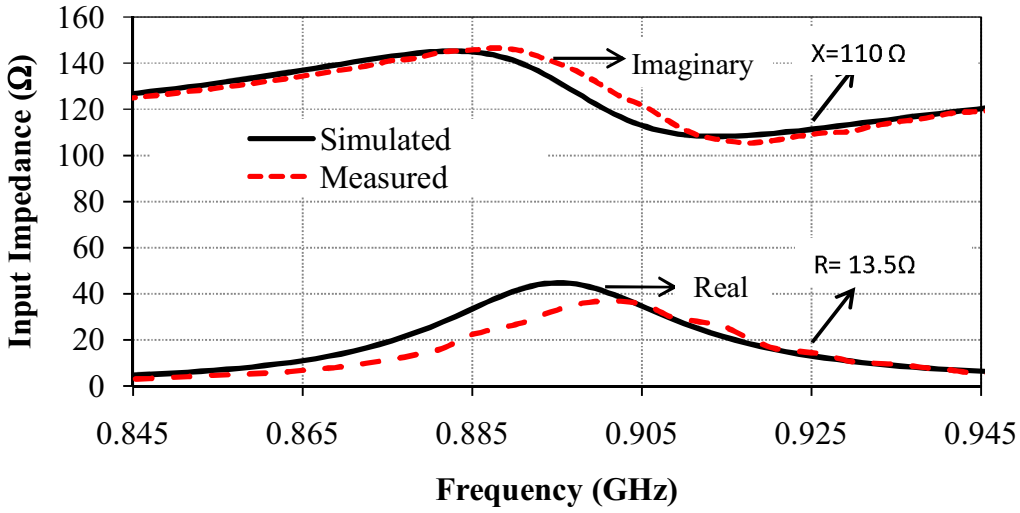

(b)

Figure 3.11: Simulated and measured (a) power reflection coefficient and (b) input impedance of proposed antenna with optimum values.

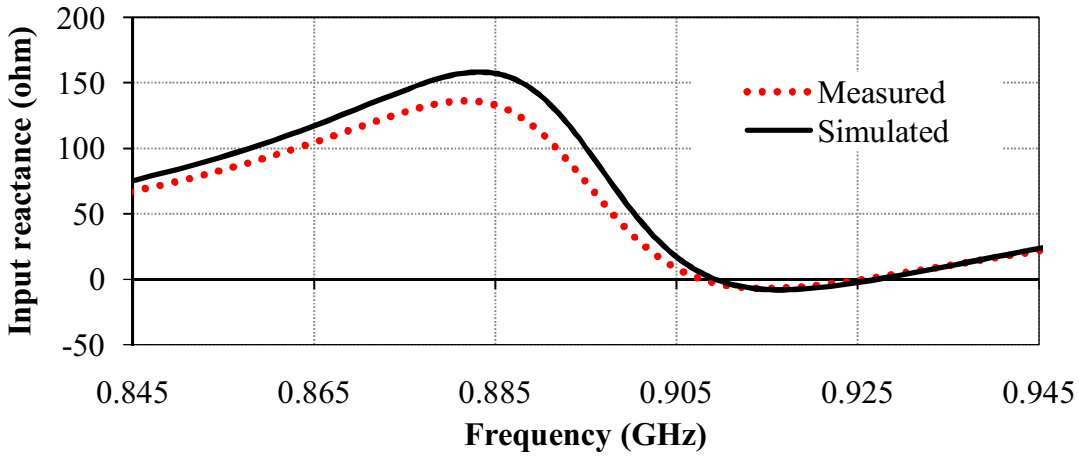

Figure 3.12: Simulated and measured input reactance of backscattered antenna with optimum values

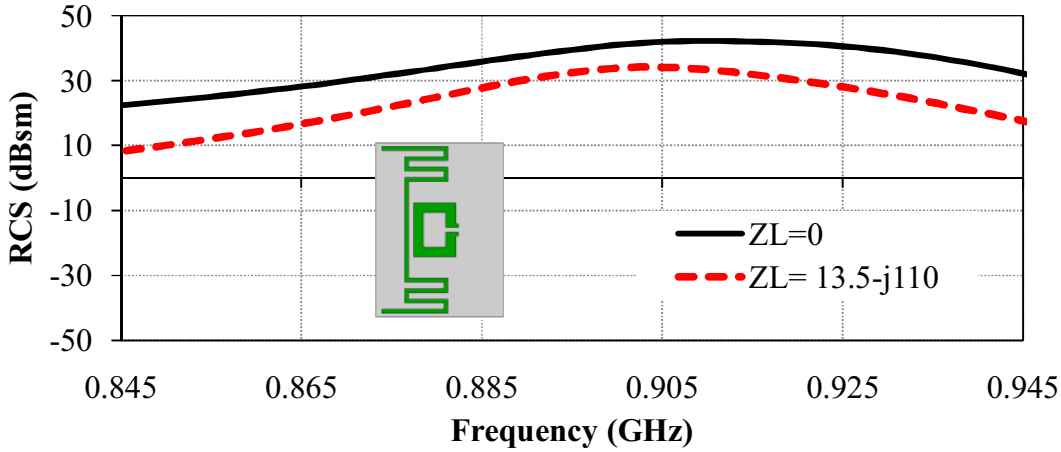

(a)

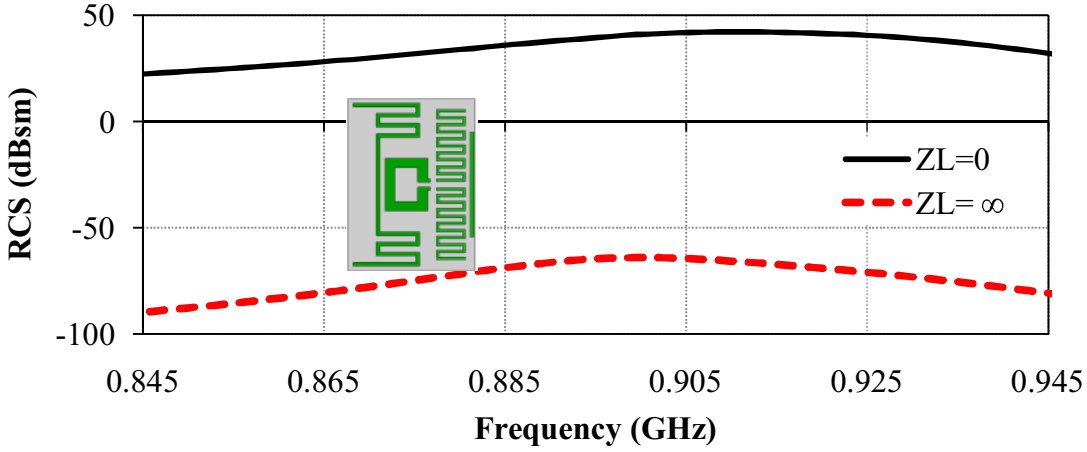

(b)

Figure 3.13: RCS of (a) conventional antenna in two states (matched and short circuit) and (b) proposed antenna in two states (open and short circuit).

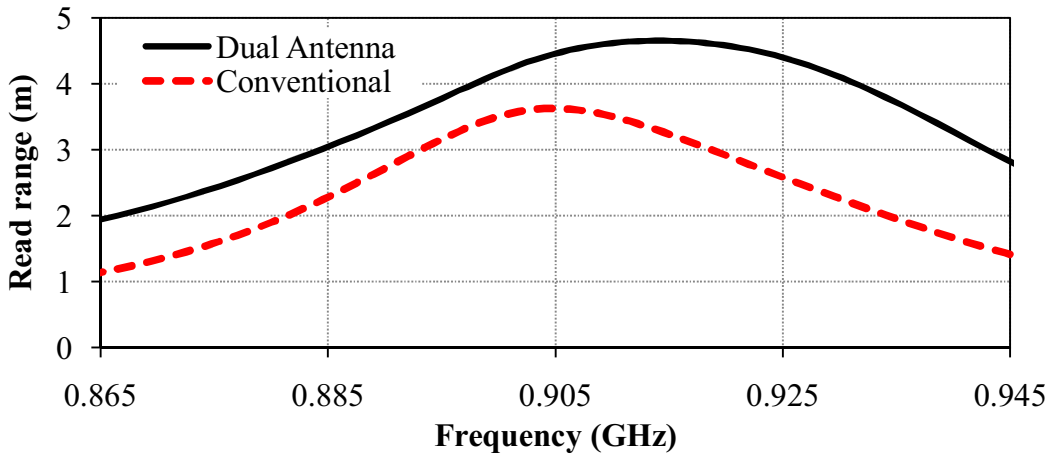

Figure 3.14: Read range comparison of conventional and proposed antenna.

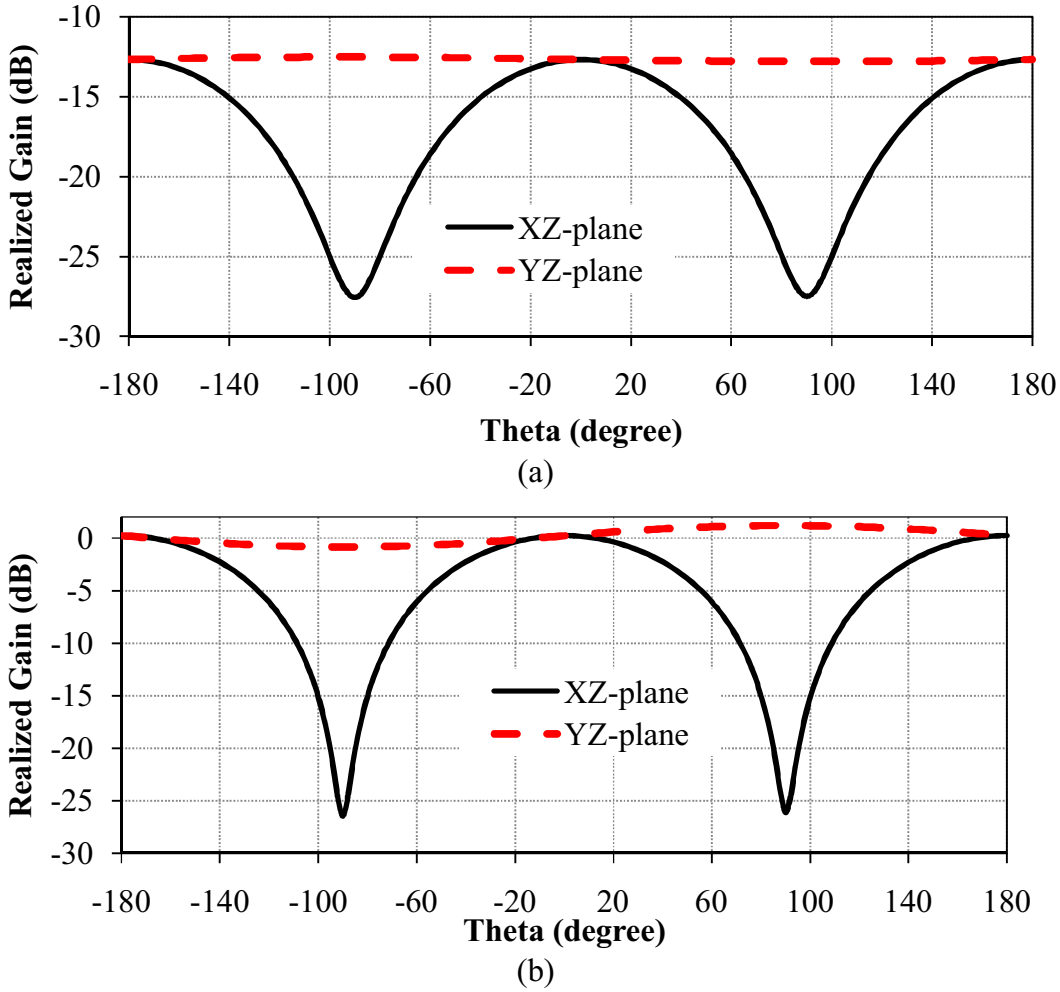

Figure 3.15: Radiation pattern of (a) Receiving antenna and (b) Backscattering antenna at 925 MHz in terms of realized gain.

Figure 3.16 shows the surface current of antenna at 925 MHz. it is observed that surface current is distributed more on driven meandered line element which is responsible for more radiation at 925 MHz.

3.3.3. Effect of mounting material on RFID tag antenna

To investigate the effect of different material on which RFID tag antenna is to be mounted, the input impedance of antenna is simulated on plastic, paper and metallic surfaces, as shown in Figure 3.17. The electrical properties for the different materials are presented in Table 3.3. It is observed that the input impedance will not change significantly on plastic and paper surfaces, but significant effect is observed when the antenna is mounted on the metallic surface. Therefore, the presented antenna is suitable for mounting on paper, card board, and plastic materials.

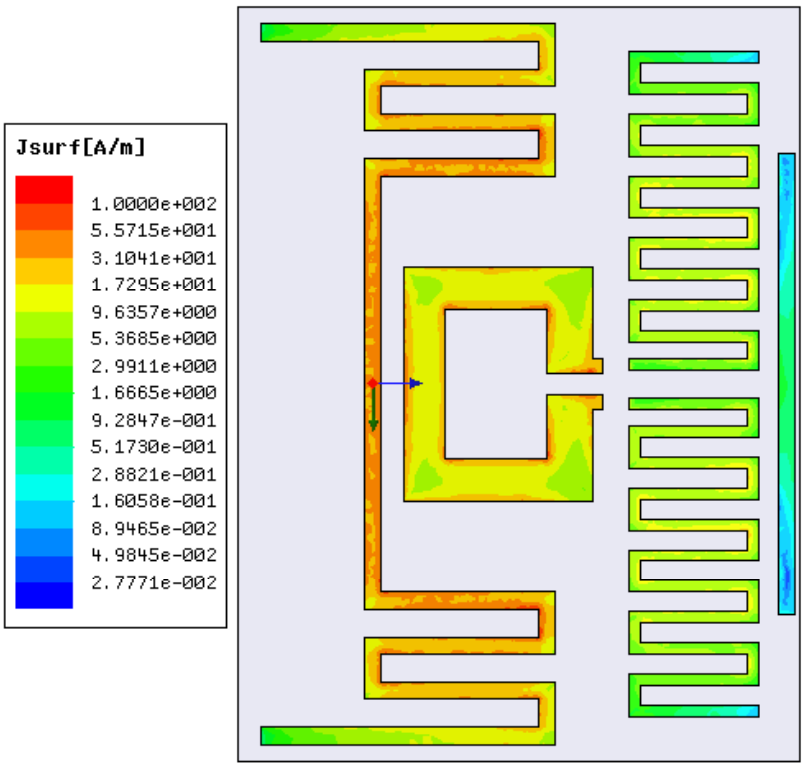

Figure 3.16: Surface current of antenna at 925 MHz

Table 3.3: Properties of different materials

Material name	Air	paper	Plastic	Metal
Relative permittivity (ε_r)	1	2.3	3.5	1
Conductivity	0	0	0	58000000

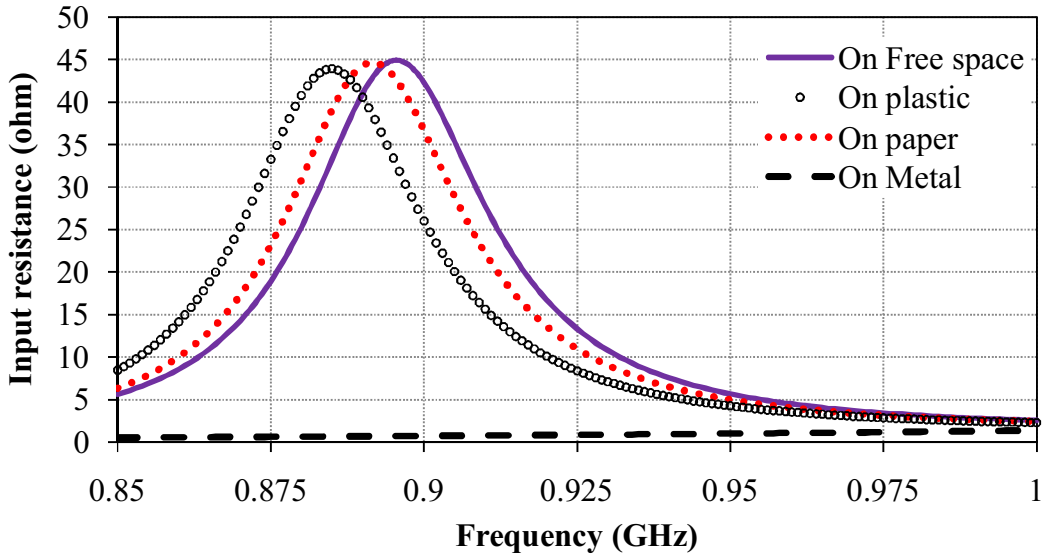

(a)

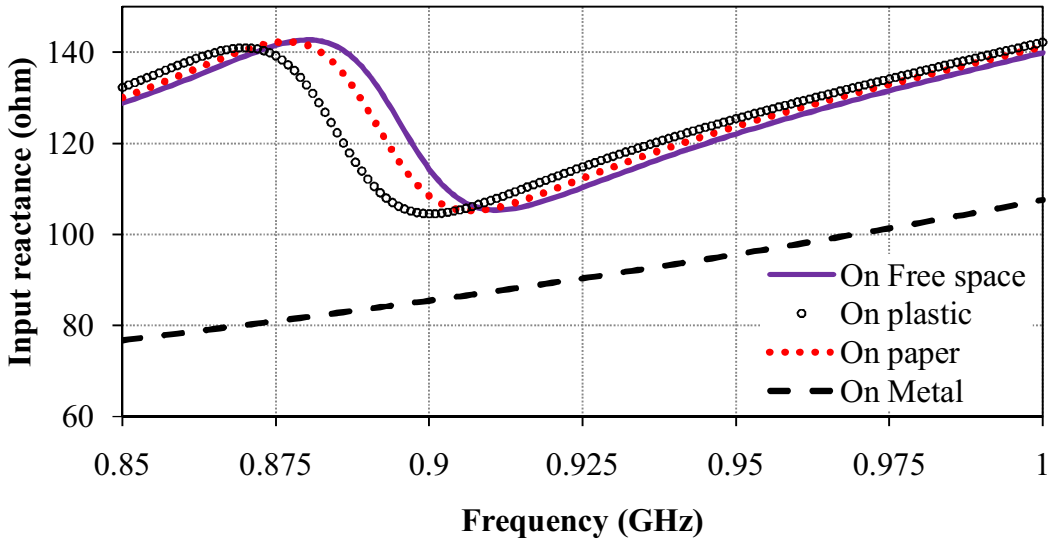

(b)

Figure 3.17: Input (a) resistance and (b) reactance of antenna on free space, plastic, paper and metal.

3.4. Summary

In this chapter, a novel meandered dual-antenna structure for UHF RFID tag is presented. Both the antennas are printed on one side of the substrate. One of the antennas is exclusively used for receiving in order to provide maximum power transfer to the tag chip. Other one is used for backscattering and designed to provide the maximum differential RCS. The design of the dual structure is discussed and the input impedance of both antennas with aid of differential technique is measured. By using the dual-antenna structure, the read range of UHF RFID system increased significantly.